Electronic Supplementary Information

Ultrathin 2D NiCo-MOF bimetallic nanosheets as single-atom catalysts for chemoselective hydrogenation of nitroarenes

Yu-Xuan Zhang[a], Yi-Jie Ma[a], Yu-Jia Zhao[a], Zi-Yan Wang[a], Cai-Xia Yu[a,*], Xiao-Qiang Li[a,*], Lei-Lei Liu[a,*]

[a] *School of Environmental and Material Engineering, Yantai University, Yantai 264005, P. R. China*

* Corresponding author. E-mail addresses: liuleileimail@163.com (L.-L. Liu).

Section 1. Materials and physical measurements

General Procedure. 1, 3, 5-benzenetricarboxylic acid (H_3BTC, 98%), benzaldehyde (99%), 4-methylbenzaldehyde (98%), 4-anisaldehyde (98%), nitrobenzene (99%) and 4-nitroanisole (98%), 5-hydroxymethyl-2-furaldehyde (97%), 4-chloronitrobenzene (4-CNB; 99.5%), 3-chloronitrobenzene (99%), 2-chloronitrobenzene (99%), 4-nitrotoluene (99%), 2-nitrotoluene (99%), 4-nitrophenol (99%), $Co(NO_3)_2{\cdot}6H_2O$ (99%) and $Ni(NO_3)_2{\cdot}6H_2O$ (98%) were obtained from Shanghai Macklin Biochemical Technology. These chemicals and reagents were obtained from commercial sources and used as received without treatment. Powder X-ray diffraction (PXRD) was performed using a PANalytical X'Pert PRO MPD system (PW3040/60). Thermal analysis was performed with a Netzsch STA-449F3 thermogravimetric analyzer at a heating rate of 10 °C min^{-1} and a flow rate of 20 cm^3 min^{-1} (N_2). Fourier transform infrared (FT-IR) spectra were recorded on an IR Prestige 21. The FT-IR samples were prepared by blending the compound with KBr and compressing the mixture to obtain transparent sheets. Scanning electron microscopy (SEM) image was observed by the JSM-7610F (JEOL, Japan) apparatus working at an acceleration voltage of 10 kV. The energy dispersive spectrometer (EDS) spectroscopy was recorded with a Bruker XFlash 6130 system at 15 kV. X-ray photoelectron spectroscopy (XPS) was measured on a Thermo Escalab 250 X-ray photoelectron spectrometer equipped with Al radiation as the probe (Kα, radiation). UV-vis diffuse reflectance spectrum (UV-vis DRS) was recorded in the spectral region of 350-800 nm with a spectrophotometer (UV-2600, Techcomp).

Preparation of $[Ni_{1.5}Co_{1.5}(BTC)_2(H_3BTC)(DMF)_3]_n$ (NiCo-MOF). $Ni(NO_3)_2{\cdot}6H_2O$ (20.4 mg, 0.07 mmol), $Co(NO_3)_2{\cdot}6H_2O$ (20.4 mg, 0.07 mmol), H_3BTC (29.4 mg, 0.14 mmol), DMF (18 mL) and one drop of HCl (0.5 mol/L) were placed in a 20 mL glass bottle. Then the bottle was sealed and kept in an oven at a temperature of 353 K for 72 h. After slow cooling down to room temperature, the bulk crystals of **NiCo-MOF** ($Ni_{0.5}Co_{0.5}$-MOF) were obtained, which were washed with DMF and dried at room temperature. The Ni_xCo_y-MOFs (Ni:Co = 1:0, 0.75:0.25, 0.25:0.75, 0:1) with different metal ratios were prepared in the same way as $Ni_{0.5}Co_{0.5}$-MOF, except using $n_{Ni(NO_3)_2{\cdot}6H_2O}$:$n_{Co(NO_3)_2{\cdot}6H_2O}$ = 1:0, 0.75:0.25, 0.25:0.75, 0:1 instead of $Ni(NO_3)_2{\cdot}6H_2O$ and $Co(NO_3)_2{\cdot}6H_2O$.

Preparation of 2D NiCo-MOF nanosheets. Firstly, the bulk **NiCo-MOF** was ground for about 1 h. Secondly, the ground MOF samples were activated by heating at 403 K (12 h) under a vacuum to remove the solvent molecules. Thirdly, the as-prepared MOF (50 mg) was dispersed in 100 mL MeOH/isopropanol (4:1, V/V) and sonicated in an ice-water bath for 6 h. After sedimentation for 12 h, the upper colloidal suspension was centrifugated at 10000 rpm at 278 K to get the exfoliated 2D MOF nanosheets, which were then collected and dried in air. The MeOH molecules

with relatively small size can readily penetrate the interlayer spaces within **NiCo-MOF**, disrupting the interlayer interactions, and the bulks MOFs can be efficiently exfoliated into MOF nanosheets through ultrasonic treatment. Isopropanol molecules, leveraging their hydroxyl groups, establish weak interactions with the surfaces of the exfoliated MOF nanosheets, and the relatively large size of isopropanol molecules can effectively prevent the re-stacking of the exfoliated MOF nanosheets. Thus, MeOH/isopropanol was chosen for the exfoliation of bulky **NiCo-MOF**.

X-ray crystal structure determination. Single X-ray diffraction intensities of crystal were collected on a D8-QUEST diffractometer at 183 K. All diffractometers were equipped with a graphite monochromated Mo-Kα radiation (λ = 0.71073). The structure was solved by the direct method and expanded with the Fourier technique. All calculations were performed with APEX-4 package. All H atoms in **NiCo-MOF** were placed in geometrically idealized positions and constrained to ride on their parent atoms. The crystal data for **NiCo-MOF** was summarized as follows: $C_{24}H_{36}CoN_2NiO_{14}$, Mr = 694.17, hexagonal, space group $P6_3/m$, a = 16.6439(12) Å, b = 16.6439(12) Å, c = 14.3100(16) Å, α = 90°, β = 90°, γ = 120°, V = 3433.1(6) $Å^3$, Z = 3, D_c = 1.007 $g·cm^{-3}$, F(000) = 1083.0 and μ = 0.819 mm^{-1}, 19442 reflections collected, 2184 unique (R_{int} = 0.1539), R_1 = 0.1105, wR_2 = 0.3378 and S = 1.222. Crystallographic data have been submitted to the Cambridge Structural Database with deposition number CCDC 2382176.

TEM and AFM characterizations. Prior to the characterizations of transmission electron microscopy (TEM) and atomic force microscopy (AFM), 3 mg of the as-prepared MOF was dispersed in 10 mL of MeOH/isopropanol (4:1, V/V) and sonicated in an ice-water bath for 6 h. After sedimentation for 12 h, the upper colloidal suspension of 2D nanosheets was dropped onto the holey carbon-coated carbon support copper grids and mica, respectively, and then naturally dried in the air. TEM images were operated at an acceleration voltage of 200 kV (JEOL JEM 2100). AFM images were obtained on a dimension edge microscope (Bruker Edge) equipped with a tapping mode.

Section 2. Catalytic experiments

Typically, 2 mmol 4-CNB and 1 mg catalyst were dispersed in 40 mL MeOH. 8 mmol $NaBH_4$ was added and the resulting mixture was stirred at room temperature. During the reaction, samples were taken at intervals until the end of the reaction. After the reaction, the samples were diluted by MeOH and tested.

Analysis of 4-CNB, 4-chloroaniline (4-CA) and aniline was made on Waters Alliance 2695 HPLC system with Waters 2687 UV detector and a reversed-phase ZORBAX Eclipse XDB-C18 column (4.6 × 250 mm). MeOH and H_2O with a volume ratio of 50:50 was used as mobile phase at a flow rate of 1.0 mL/min, and the wavelength was 254 nm. The content of 4-CNB, 4-CA and aniline in the product solution was directly obtained by the calibration curve of external standard constructed by pure substance, and the conversion, selectivity and yield were calculated. Conversion of 4-CNB, selectivity and yield of 4-CA were defined as follows:

$$\text{Conversion} = \frac{n_{4\text{-CNB},0} - n_{4\text{-CNB},t}}{n_{4\text{-CNB},0}} \times 100\ \%$$

$$\text{Selectivity} = \frac{n_{4\text{-CA},t}}{n_{4\text{-CNB},0} - n_{4\text{-CNB},t}} \times 100\ \%$$

$$\text{Yield} = \frac{n_{4\text{-CA},t}}{n_{4\text{-CNB},0}} \times 100\ \%$$

where $n_{4\text{-CNB},0}$ (mmol) and $n_{4\text{-CNB},t}$ (mmol) are amount of substance 4-CNB at time 0 (min) and at any time t (min); $n_{4\text{-CA},t}$ (mmol) is amount of substance 4-CA at any time t (min).

Section 3. Calculation method

Adsorption model calculation. In order to better explain the reaction mechanism, the DMol[3] module in Materials Studio was used to perform simulations based on density-functional theory (DFT). A combination of generalized gradient approximation (GGA) and Perdew-Burke-Ernzerhof (PBE) generalized function was used for the calculations, the basis set was selected as dual-valued orbital basis set + d-orbital polarization function (DND). The iteration error of the self-consistent field (SCF) was set to 1.0×10^{-5} Ha, and the convergence criterion for the structure optimization and the total energy calculations was set to 2.0×10^{-5} Ha. The maximum force and maximum displacement were set to 0.004 Ha/Å and 0.005 Å, respectively. The maximum number of SCF turns was set to 150, smearing was set to 0.025, and the solvation model was methanol.[1, 2] The Gibbs free energy was calculated considering only the numerical differences in adsorption, and the formula is as follows:

$$\Delta G_{ads} = G_{MOF + compound} - G_{MOF} - G_{compound}$$

where $G_{MOF + compound}$, G_{MOF}, and $G_{compound}$ represent the total energies of the MOF + compound system, MOF, and compound respectively. Compound = 4-CNB or 4-CA.

Reaction pathway calculation.[3] The DMol3 module in Materials Studio was used to perform simulations based on DFT. A combination of GGA-PBE generalized function was used for the calculations, the basis set was selected as DND. The iteration error of the SCF was set to 1.0×10^{-5} Ha, and the convergence criterion for the structure optimization and the total energy calculations was set to 2.0×10^{-5} Ha. The maximum force and maximum displacement were set to 0.004 Ha/Å and 0.005 Å, respectively. The maximum number of SCF turns was set to 150, smearing was set to 0.03, and the solvation model was methanol. The change in potential energy was calculated considering only the numerical differences in adsorption, and the formula is as follows:

$$\Delta E_{barrier} = E_{MOF + product} - E_{MOF + 4\text{-}CNB + H_2}$$

where $\Delta E_{barrier}$, $E_{MOF + product}$, and $E_{MOF + 4\text{-}CNB + H_2}$ represent the total energies of the reaction energy barrier, product, and reactants respectively. Product = intermediate or final product.

Section 4. Supporting Table

Table S1. Comparison of turnover frequency (TOF) in different metal based catalytic systems for 4-nitrophenol reduction.

Entry	Catalyst	TOF (min^{-1})	Reference
1	Fe-Ni NP's	0.056	4
2	Pt@Ag coreshell	0.088	5
3	Pd/FTO	0.485	6
4	Pd/C	0.792	7
5	Pd/Co@NC	0.815	8
6	Ag NPs@SCOF	1.353	9
7	Pt@CeO_2/RGO	1.44	10
8	Re-Au@MSNS	1.533	11
9	Pt-EMSiO_x	1.88	12
10	Pd/NHPC	2.045	13
11	Pt_3Au_1-PDA/RGO	3.333	14
12	Pd@PANI-CS-Fe_3O_4	3.812	15
13	AuPd/GNS	14.1	16
14	Pd@PC-POP	28.957	17
15	Au/RA-MC	30.7	18
16	Pd NPs	120	19
17	Co-MOF@$Pd_{0.0012}$	163.333	7
18	**NiCo-MOF nanosheets**	231.162	**this work**

The TOF was measured at ~100% conversion level and calculated in the format of $mol_{4\text{-aminophenol}}/(mol_{total\ metal} \cdot min_{reaction\ time})$.[20]

Section 5. Supporting Figures

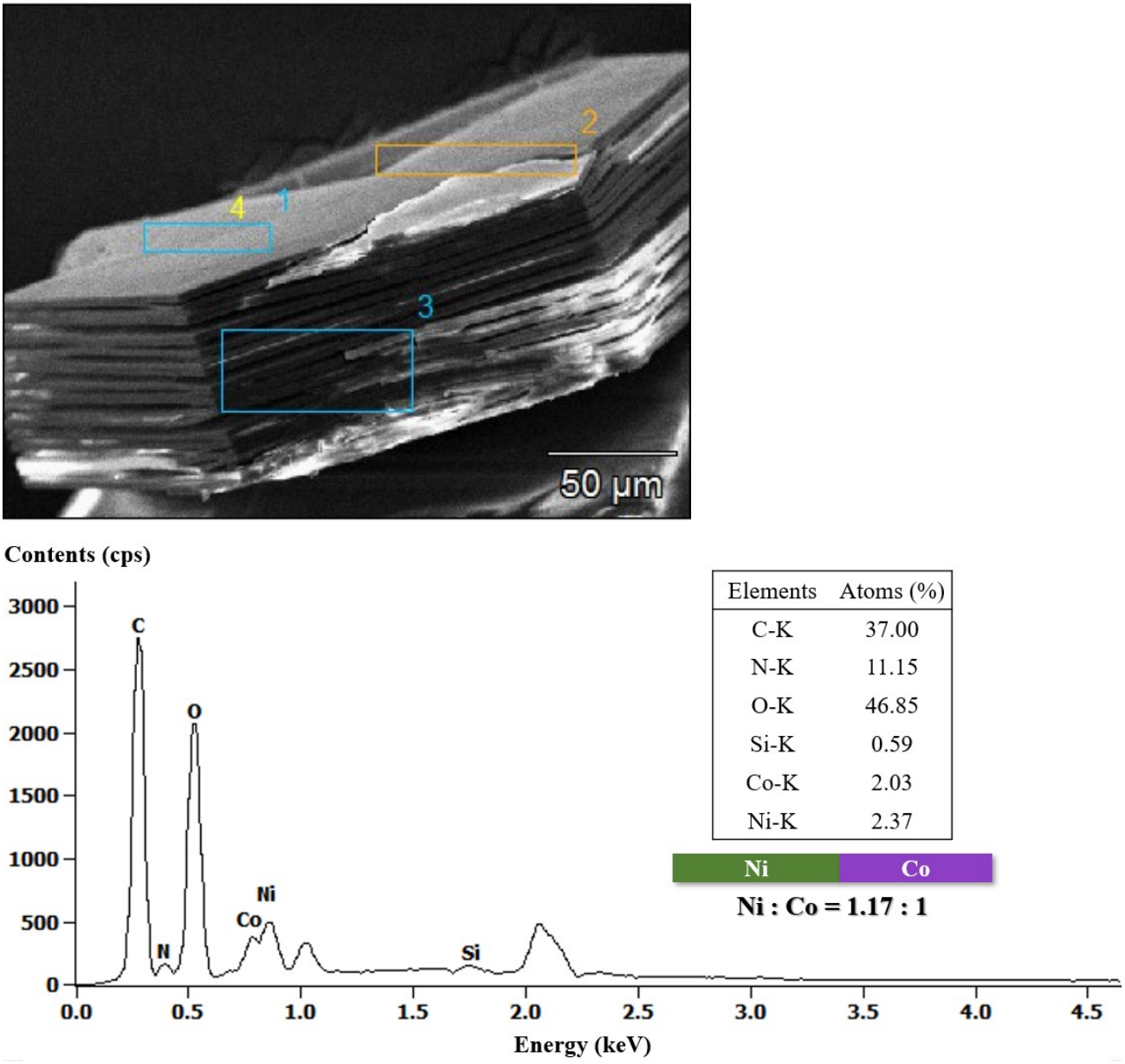

Figure S1. SEM-EDS mapping image of **NiCo-MOF**.

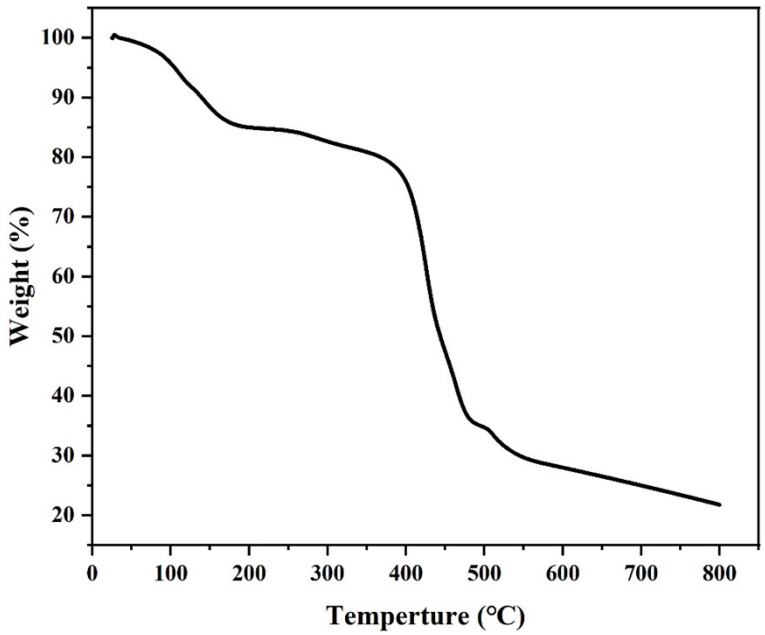

Figure S2. TGA curve of 3D bulky **NiCo-MOF**.

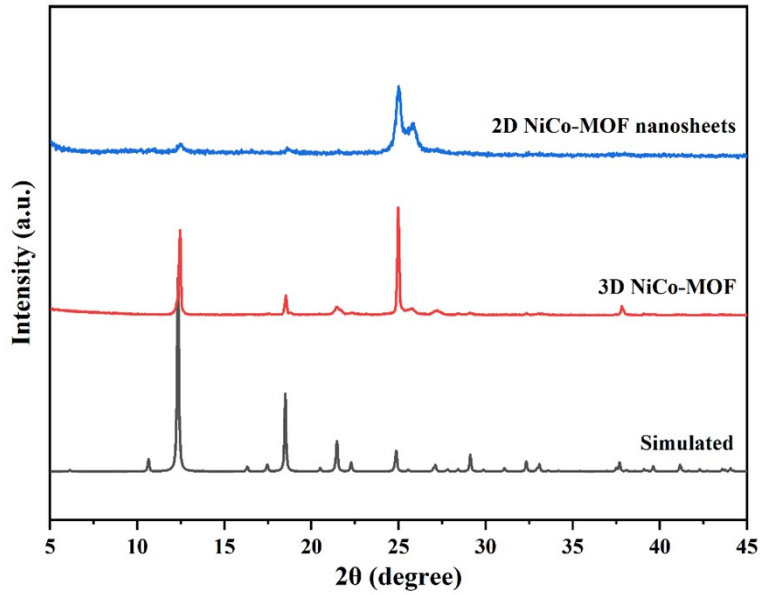

Figure S3. PXRD patterns of the simulated **NiCo-MOF**, 3D bulky **NiCo-MOF**, and 2D **NiCo-MOF** nanosheets.

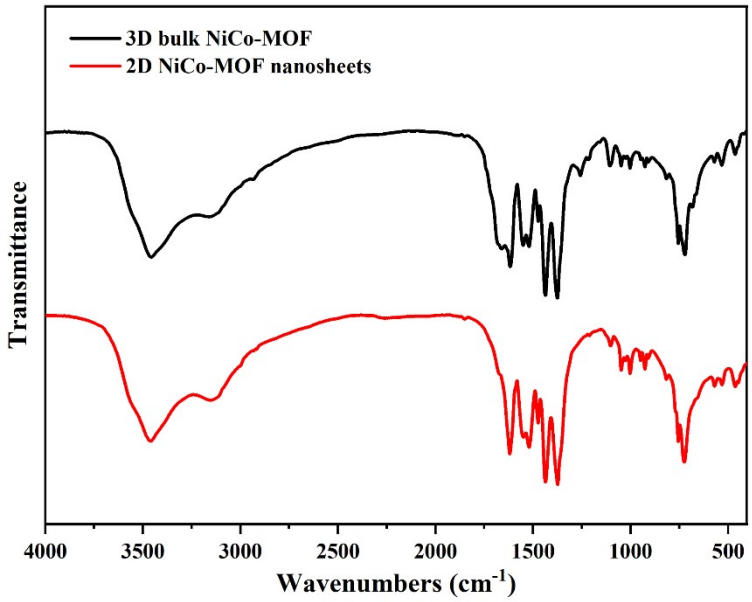

Figure S4. FT-IR spectrum of 3D bulk **NiCo-MOF** and 2D **NiCo-MOF** nanosheets.

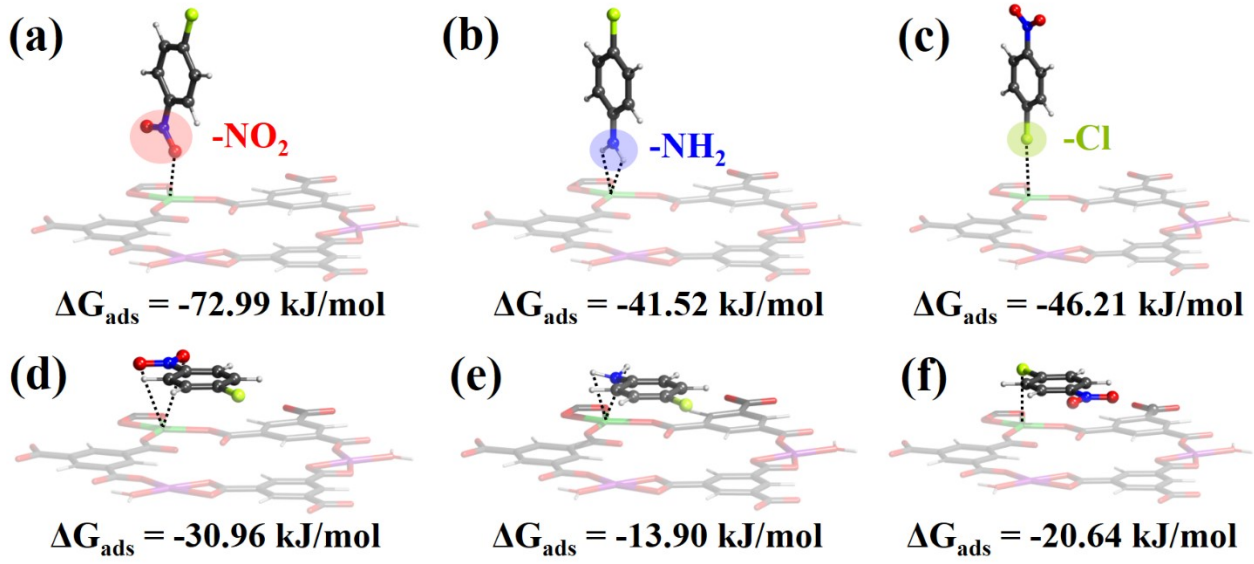

Figure S5. Adsorption configurations of 4-CNB and 4-CA on **NiCo-MOF**, and corresponding adsorption energies. Vertical adsorption of 4-CNB via -NO_2 (a), 4-CA (b), and 4-CNB via -Cl (c). Horizontal adsorption of 4-CNB via -NO_2 (d), 4-CA (e), and 4-CNB via -Cl (f).

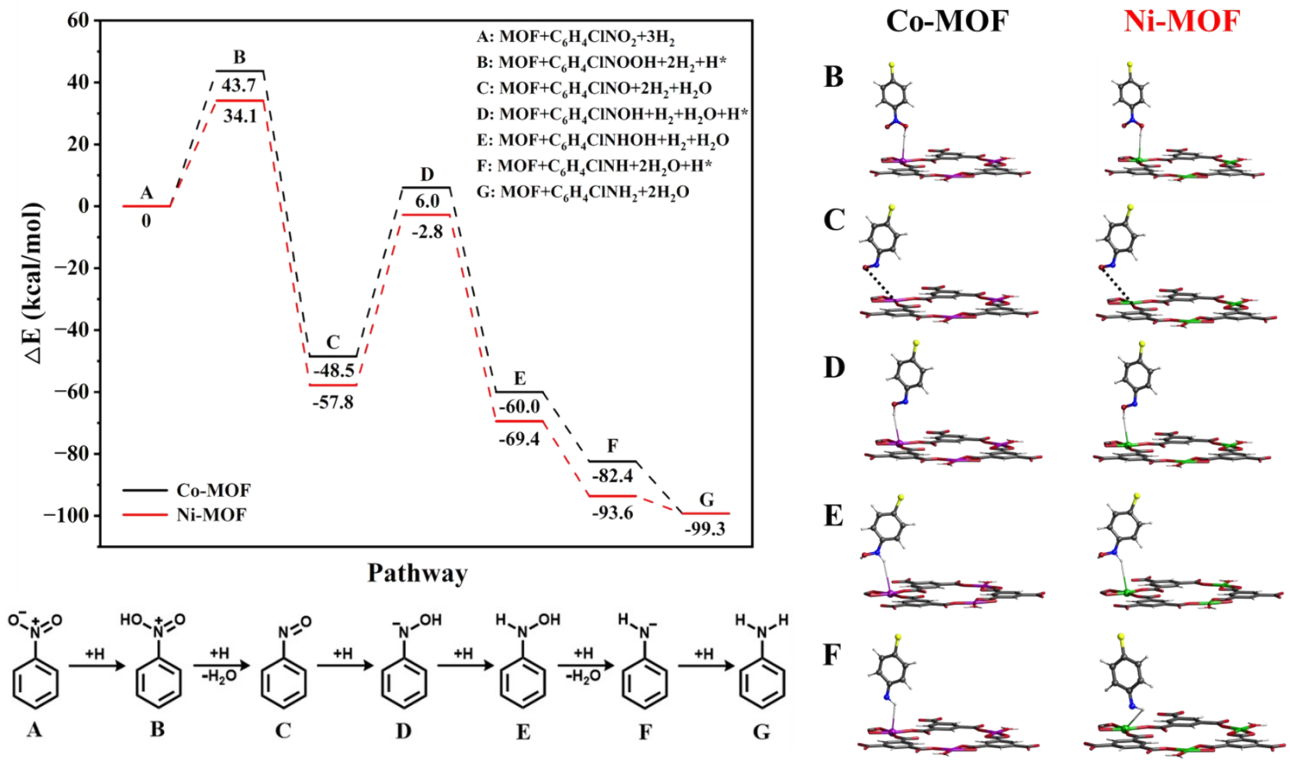

Figure S6. Potential barrier diagram of the 4-CNB reduction pathway, and Geometric configurations of reactant, intermediates and product in the process of the 4-CNB reduction after optimization.

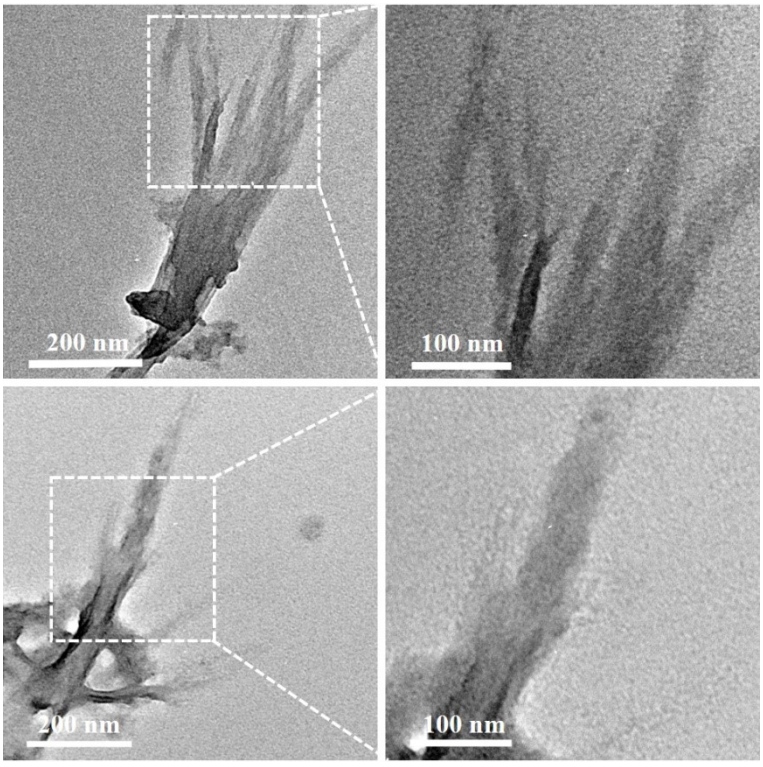

Figure S7. TEM images of the **NiCo-MOF** nanosheets after catalytic reaction.

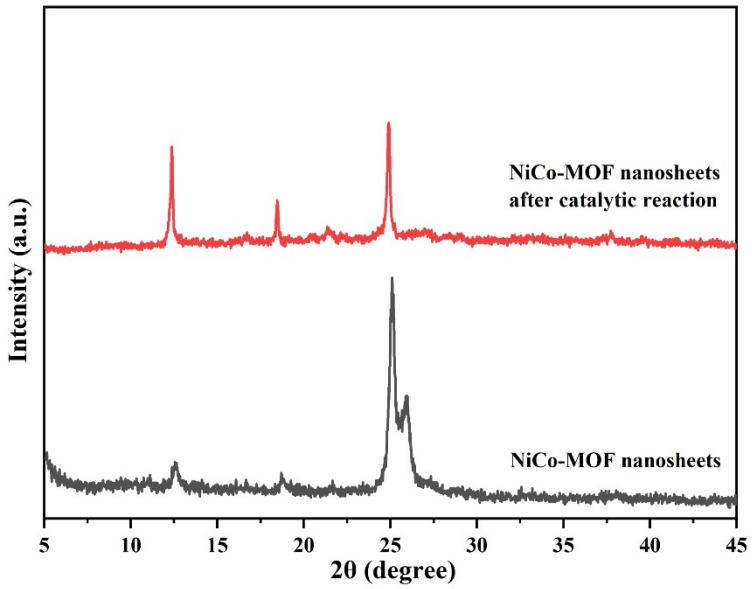

Figure S8. PXRD patterns of the **NiCo-MOF** nanosheets before and after catalysis.

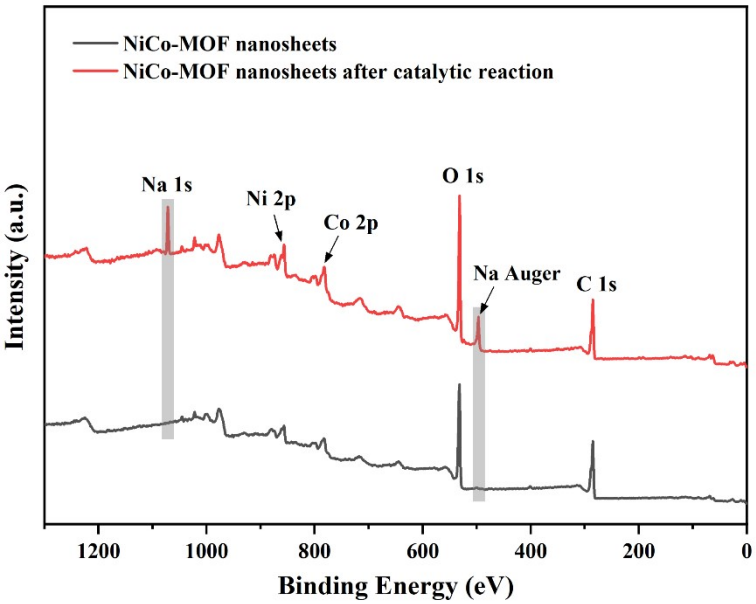

Figure S9. XPS survey spectrum of **NiCo-MOF** nanosheets before and after catalysis. The two newly emerging peaks at 1071.79 and 497.05 eV in the XPS spectrum of **NiCo-MOF** nanosheets after catalysis were attributed to Na^+ ions, as sodium borohydride decomposes into active hydrogen, borate ions and sodium ions during the catalytic process, wherein the Na^+ ions could be partially adsorbed by the uncoordinated carboxylate oxygen atoms within the MOF nanosheets.

Section 6. Supporting References

1 L. Kong and B. Shen, *Chin. J. Catal.*, 2015, **36**, 1017-1022.

2 J. Zou and X. Ren, *New J. Chem.*, 2023, **47**, 14408-14417.

3 F. Huang, Y. Deng, Y. Chen, X. Cai, M. Peng, Z. Jia, J. Xie, D. Xiao, X. Wen, N. Wang, Z. Jiang, H. Liu and D. Ma, *Nat. Commun.*, 2019, **10**, 4431.

4 D. R. Petkar, B. S. Kadu and R. C. Chikate, *RSC Adv.*, 2014, **4**, 8004.

5 Z.-S. Lv, X.-Y. Zhu, H.-B. Meng, J.-J. Feng and A.-J. Wang, *J. Colloid Interface Sci.*, 2019, **538**, 349-356.

6 S. Y. Mak, K. H. Liew, C. C. Chua, M. A. Yarmo, B. H. Yahaya, W. Z. Samad, M. S. M. Jamil and R. M. Yusop, *J. Chem. Sci.*, 2019, **131**, 111.

7 X. Duan, A. Liu, L. Zhou and S. Wei, *Environ. Sci. Pollut. Res.*, 2023, **30**, 97936-97947.

8 F. Han, Y. Zhang, H. Zhang, H. Feng, Y. Tang and X. Yang, *ChemCatChem*, 2022, **14**, e202201179.

9 N. Wang, F. Wang, F. Pan, S. Yu and D. Pan, *ACS Appl. Mater. Interfaces*, 2021, **13**, 3209-3220.

10 X. Wang, D. Liu, S. Song and H. Zhang, *J. Am. Chem. Soc.*, 2013, **135**, 15864-15872.

11 Q. Zhang, H. B. Xu, L. Pan, A. Kuchmizhak and L. Wang, *Appl. Organomet. Chem.*, 2023, **37**, e6962.

12 N. K. R. Bogireddy, P. Sahare, U. Pal, S. F. O. Méndez, L. M. Gomez and V. Agarwal, *Chem. Eng. J.*, 2020, **388**, 124237.

13 X. X. Wu and H. Zhou, *New J. Chem.*, 2017, **41**, 10245-10250.

14 W. Ye, J. Yu, Y. Zhou, D. Gao, D. Wang, C. Wang and D. Xue, *Appl. Catal. B Environ.*, 2016, **181**, 371-378.

15 M. M. Ayad, W. A. Amer and M. G. Kotp, *Mol. Catal.*, 2017, **439**, 72-80.

16 X. Chen, Z. Cai, X. Chen and M. Oyama, *J. Mater. Chem. A*, 2014, **2**, 5668-5674.

17 M. Yuan, R. Yang, S. Wei, X. Hu, D. Xu, J. Yang and Z. Dong, *J. Colloid Interface Sci.*, 2019, **538**, 720-730.

18 X. Yang, P. Lu, L. Yu, P. Pan, A. A. Elzatahry, A. Alghamdi, W. Luo, X. Cheng and Y. Deng, *Adv. Funct. Mater.*, 2020, **30**, 2002488

19 F. Liu, X. Liu, F. Chen and Q. Fu, *J. Colloid Interface Sci.*, 2021, **604**, 281-291.

20 L. Xiao, C. Cheng, Z. Li, C. Zheng, J. Du, M. Song, Y. Wan, S. Li, G. Jun and M. Zhao, *Nano Res.*, 2023, **16**, 11334-11341.